Magnetic Resonance Imaging of Radiation Injury to the Brain

John T. Curnes, D. Wayne Laster, Marshall R. Ball, Dixon M. Moody and Richard L. Witcofski

AJNR Am J Neuroradiol 1986, 7 (3) 389-394
http://www.ajnr.org/content/7/3/389

Magnetic Resonance Imaging of Radiation Injury to the Brain

John T. Curnes[1]
D. Wayne Laster[2]
Marshall R. Ball[2]
Dixon M. Moody[2]
Richard L. Witcofski[2]

Nine patients with a history of radiation of 2400–6000 rad (24–60 Gy) to the brain were examined by magnetic resonance imaging (MRI) and computed tomography (CT). MRI demonstrated abnormalities in the periventricular white matter in all patients. The abnormal periventricular signal was characterized by a long T2 and was demonstrated best on coronal spin-echo (SE) 1000/80 images. A characteristic scalloped appearance at the junction of the gray-white matter was seen on MR images of seven patients, and represented extensive white-matter damage involving the more peripheral arcuate fiber systems. This differs from transependymal absorption, which is seen best on SE 3000/80 images and has a smooth peripheral margin. Cranial CT demonstrated white-matter lucencies in six cases but generally failed to display the extent of white-matter injury demonstrated by MRI. MRI is uniquely suited to detect radiation injury to the brain because of its extreme sensitivity to white-matter edema.

Recent reports show increased awareness and detection of intracranial radionecrosis after radiation therapy to a primary or secondary malignancy [1–3]. Nevertheless, the incidence of this complication of radiotherapy remains surprisingly low considering the inevitable exposure of normal brain tissue to the radiation beam.

Cranial computed tomography (CT) is currently the procedure of choice in detecting postradiation complications; however, magnetic resonance imaging (MRI) shows greater sensitivity in the detection of white-matter disease [4]. We report a comparison of concurrent MRI and CT findings in nine patients previously treated with 2400–6000 rad (24–60 Gy) total radiation.

Materials and Methods

A retrospective review of the medical records and neuroradiologic studies in nine patients with a history of radiation therapy to the brain was performed. All patients received whole-brain irradiation. Subjects included seven males and two females with an age range of 11–70 years. Clinical histories and radiologic findings are summarized in Table 1. The diagnosis was pathologically proven only in case 2. All patients had symptoms varying in severity from lethargy and confusion to seizures and ataxia. All but one patient received chemotherapy in addition to cranial irradiation (Table 1). Four cases of noncommunicating hydrocephalus were reviewed retrospectively to determine if there is a characteristic pattern to transependymal absorption. In all four cases, benign posterior fossa tumors obstructed the aqueduct or fourth ventricle.

MR studies were performed on a resistive-magnet prototype imager manufactured by Picker International (Picker 1000) and operating at a frequency of 6.4 MHz with a magnetic field of 0.15 T (1500 G). A 30 cm aperture was used. Images in the transverse, sagittal, and coronal planes were obtained with three pulse sequences: inversion recovery (IR) using a 1400 msec repetition time (TR) and a 400 msec inversion time (TI), and spin-echo (SE) using both 1000 msec and 3000 msec TR and 80 msec echo delay time (TE). Patients were studied with either four, eight, or 16 contiguous 1 cm slices. Images were generated by filtered-back projection or two-dimensional Fourier transform on a 256 × 256 matrix.

CT scans were obtained on either an EMI 1005 (160 × 160 matrix) scanner or a General

This article appears in the May/June 1986 issue of *AJNR* and the July issue of *AJR*.

Received May 23, 1985; accepted after revision October 8, 1985.

[1] Department of Radiology, University of North Carolina School of Medicine, Chapel Hill, NC 27514.

[2] Department of Radiology, Bowman Gray School of Medicine, Wake Forest University, 300 S. Hawthorne Rd., Winston-Salem, NC 27103. Address reprint requests to D. W. Laster.

***AJNR* 7:389–394, May/June 1986**
0195–6108/86/0703–0389

TABLE 1: **Clinical and Radiographic Findings in Radiation Injury to the Brain**

Case No. (age, gender), Primary Diagnosis	Total Cumulative Brain Radiation Dose (rad)/ Days	Latency (months)	Chemotherapy/No. of Courses	CT Findings	MRI Findings
1 (41, M), Astrocytoma grade II	6000/42	48	Cis-platinum/10	Cerebral atrophy, white-matter edema	Cerebral atrophy, scalloped white-matter edema, symmetric
2 (56, M), Glioblastoma multiforme	5500/49	28	BCNU/5	Cerebral atrophy, focal enhancing masses, white-matter edema	Cerebral atrophy, focal areas with long T2 scalloped white-matter edema, asymmetric, some gray-matter involvement
3 (42, M), Astrocytoma grade II	6000/42	72	BCNU/10	Normal	Scalloped white-matter edema, asymmetric
4 (70, F), Colon adenocarcinoma; metastasis to brain	3000/10	3	Methotrexate/3	Cerebral atrophy, white matter edema	Cerebral atrophy, scalloped white-matter edema, asymmetric
5 (44, M), Nasopharyngeal squamous cell carcinoma eroding skull base	3500/49	10	Methotrexate, cytoxan/5	Mild cerebral atrophy, no white-matter edema	Scalloped white-matter edema, asymmetric
6 (70, M), Lung small cell carcinoma; prophylactic treatment	3000/10	24	Methotrexate/15	Normal	Irregular white-matter edema, asymmetric
7 (18, M), Pineocytoma	5500/42	18	None	Cerebral atrophy	Irregular white-matter edema, asymmetric
8 (11, M), Acute lymphocytic leukemia	2400/10	24	Methotrexate, prednisone, VP-16, vincristine/>50; also, intrathecal methotrexate/20	Cerebral atrophy, white-matter edema, mineralizing microangiopathy	Cerebral atrophy, scalloped white-matter edema
9 (56, F), Lung small cell carcinoma; prophylactic treatment	3000/10	18	Methotrexate/15	Normal	Scalloped white-matter edema, asymmetric

Electric CT/T 8800 CT scanner. Pre- and postinfusion scans were obtained in all cases. Enhancement was produced by the intravenous drip infusion of 300 ml of 30% Renografin.

Results

Table 1 summarizes the clinical information and compares the CT and MRI findings for the patients studied. CT scans obtained before and during the course of radiation therapy demonstrated progressive ventricular dilatation and cortical atrophy in six patients. Periventricular lucencies, manifest as decreased attenuation of the white matter, were seen on postradiation CT scans in five of the six (Fig. 1). Three other patients had normal CT scans (Fig. 2). In contrast, MRI demonstrated abnormalities of the periventricular white matter in all subjects, and, where CT detected periventricular lucencies, MRI demonstrated additional areas of involvement (Figs. 1–4).

Coronal SE 1000/80 images provided optimal contrast between the gray matter, abnormal white matter, and ventricular cerebrospinal fluid (CSF). Abnormal white matter was seen well on axial SE 3000/80 images, but contrast between the abnormal white matter and the ventricular CSF was lost since T2 is long for both entities (Fig. 3). The IR 1500/40 pulse sequence did not provide the contrast necessary for detection of abnormal white matter.

Two basic patterns for MRI of radiation injury emerged: a scalloped appearance reflecting damage throughout the white matter including the arcuate (U) fibers (Figs. 1 and 3); and a less extensive, irregular periventricular signal that was asymmetric (Fig. 2). The corpus callosum was spared in all cases.

Histologic brain examination at autopsy in case 2 revealed areas of fluffy, chronic edema extending throughout the white-matter fiber tracts (Figs. 4D and 4E). Radiation-induced hyalinization and fibrinoid necrosis of the blood vessels were prominent. Areas of radiation necrosis were present. Extensive demyelination was noted. Residual tumor was found only in the surgical bed.

In all cases of transependymal absorption, the abnormal signal was best seen on SE 3000/80 axial images. The peripheral margin was more difficult to see on coronal SE 1000/80 images, but in all cases appeared smooth and symmetric (Fig. 5).

Discussion

Courville and Myers [5] found the effects of radiation to be primarily thickening and hyalinization of the arteriolar wall. Evidence suggesting that the associated demyelination re-

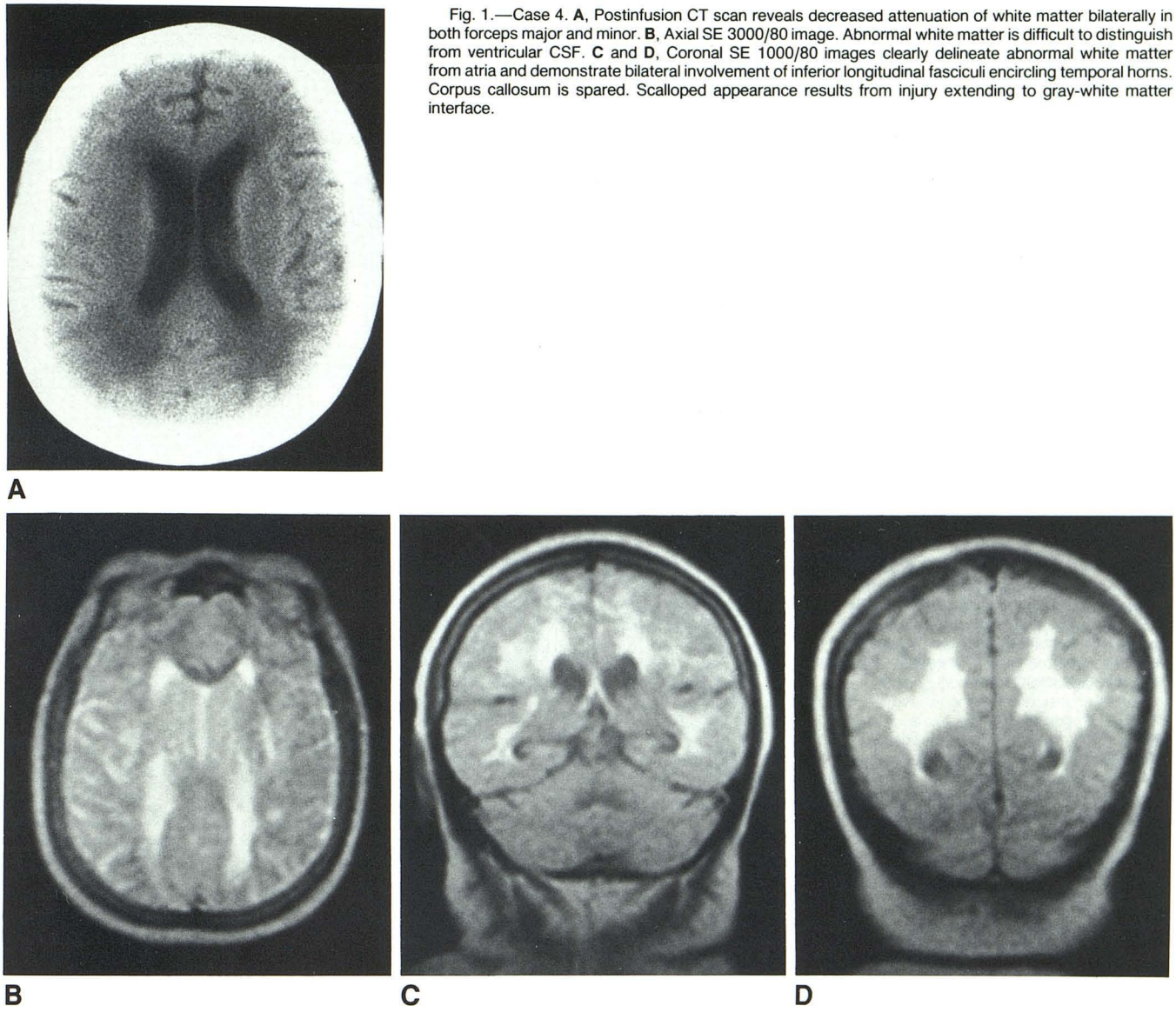

Fig. 1.—Case 4. **A**, Postinfusion CT scan reveals decreased attenuation of white matter bilaterally in both forceps major and minor. **B**, Axial SE 3000/80 image. Abnormal white matter is difficult to distinguish from ventricular CSF. **C** and **D**, Coronal SE 1000/80 images clearly delineate abnormal white matter from atria and demonstrate bilateral involvement of inferior longitudinal fasciculi encircling temporal horns. Corpus callosum is spared. Scalloped appearance results from injury extending to gray-white matter interface.

sults from the vascular changes includes a long interval preceding the onset of symptoms, fibrinoid changes in arteriolar walls in the affected area, the severest changes in the white matter occurring in deep locations adjacent to the ventricle where blood supply is most tenuous, and high correlation between the severity of vascular change and the severity of demyelination.

In case 2, hyalinized blood vessels and demyelination were accompanied by chronic, interstitial edema and vacuolization of the interstitium. These findings were present in the white matter remote from the areas of radiation necrosis. Reactive astrocytic changes associated with the edema indicate a chronic rather than acute process. This alteration of normal white-matter composition with increased extracellular brain water and loss of myelin accounts primarily for the long T2 signal seen in radiation damage.

The abnormal MRI signal seen in transependymal absorption from obstructive hydrocephalus differs from that of radiation-injured white matter. The white-matter changes seen in hydrocephalus appear on CT as a linear decrease in hypodensity from ventricle to periphery. On MRI, the abnormally prolonged T2 signal extending outward from the (microscopically) disrupted ventricular wall also decreases linearly. It has a round, smooth contour, does not extend to the gray-white matter junction, and typically spares the centrum semiovale [6]. In contrast, radiation injury is irregular and flame-shaped, extending to the more richly vascular gray matter in severe cases, and affecting all white-matter fiber tracts except the corpus callosum. The forceps major was more severely affected in some cases than the more anterior white-matter tracts. This may reflect the fact that the penetrating arterioles posteriorly must traverse a longer course to penetrate the thicker fiber bundles in this area, while tracts of the corpus callosum are fed directly by short perforators from pial arteries

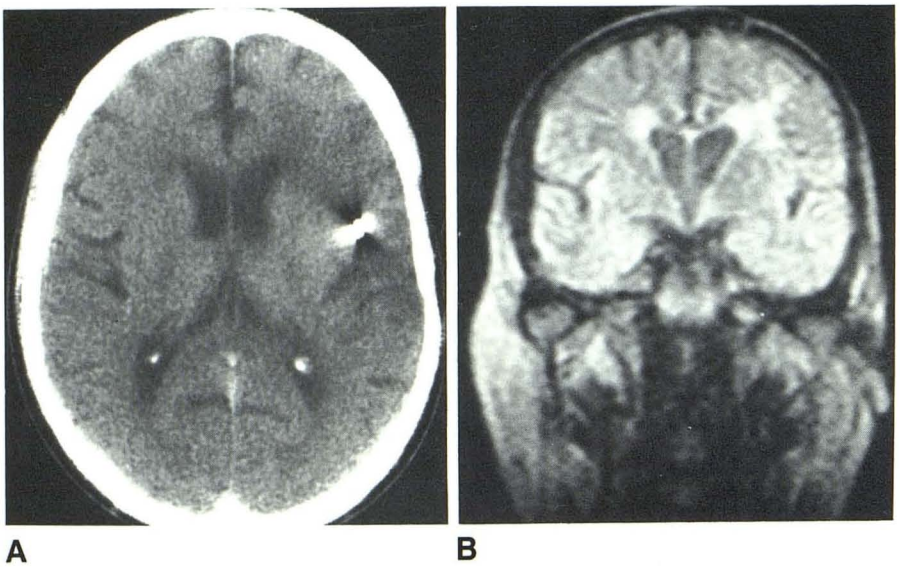

Fig. 2.—Case 3. **A**, Postinfusion CT scan shows no white-matter abnormalities. Mild ventricular enlargement and cortical atrophy. Surgical clip marks operative site. **B**, Coronal SE 1000/80 image. Moderate white-matter damage with asymmetric, irregular periventricular signal. Note contrast between involved white matter, dark gray matter, and darker CSF.

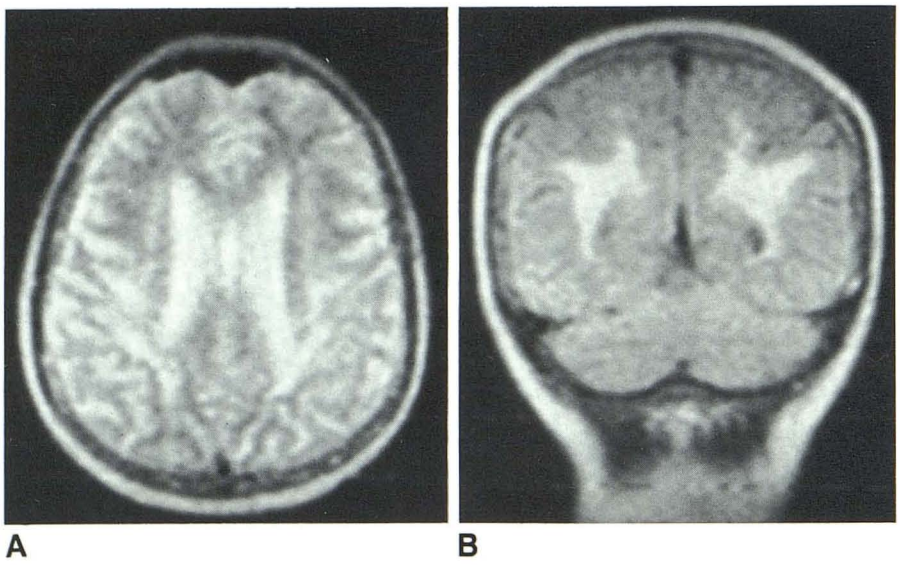

Fig. 3.—Case 9. **A**, Axial SE 3000/80 section through centrum semiovale poorly demonstrates abnormal white-matter signal. **B**, Coronal SE 1000/80 image demonstrates abnormal white matter posteriorly. Characteristic scalloped appearance results from involvement of arcuate (U) fiber tracts that abut gray matter.

such as the anterior cerebral arteries and posterior pericallosal arteries.

The influence of fiber tracts on the distribution and appearance of cerebral edema has been shown by Cowley [7]. Our study confirms his observation that the corpus callosum is the only white-matter fiber tract immune from involvement with diffuse edema. In case 4 (Fig. 1), MRI was superior to CT in its ability to delineate the inferior longitudinal fasciculi surrounding the temporal horns. The characteristic scalloped MRI appearance arises from damage to the arcuate (U) fibers, which interconnect the gyri and abut the gray matter (Fig. 3).

Coronal SE 1000/80 slices optimally display white-matter injury for two reasons. First, the coronal plane profiles the abnormal fiber bundles against two normal tissues, the richly vascular gray matter and the ventricular CSF. Second, the SE 1000/80 sequence produces the greatest contrast between these three structures. Axial SE 3000/80 slices fail to display the lesions as well because the T2 signal from injured white matter is similar to that of CSF and provides little contrast between CSF and the ventricle.

The differing appearance of radiation injury and transependymal absorption on T2-weighted (SE 3000/80) and T1-weighted (SE 1000/80) images reflect their different etiologies. In transependymal absorption, breakdown of the ventricular lining causes egress of CSF into the fiber tracts, whereas in radiation injury, demyelination, interstitial edema, and even tissue necrosis are seen. Currently, calculation of T1 and T2 values for radiation injury and transependymal absorption are being studied. Dooms et al. [8] found nonspecific prolongation of T1 and T2 in radiation-injured white matter.

Ventricular dilatation resulting from radiation-induced cere-

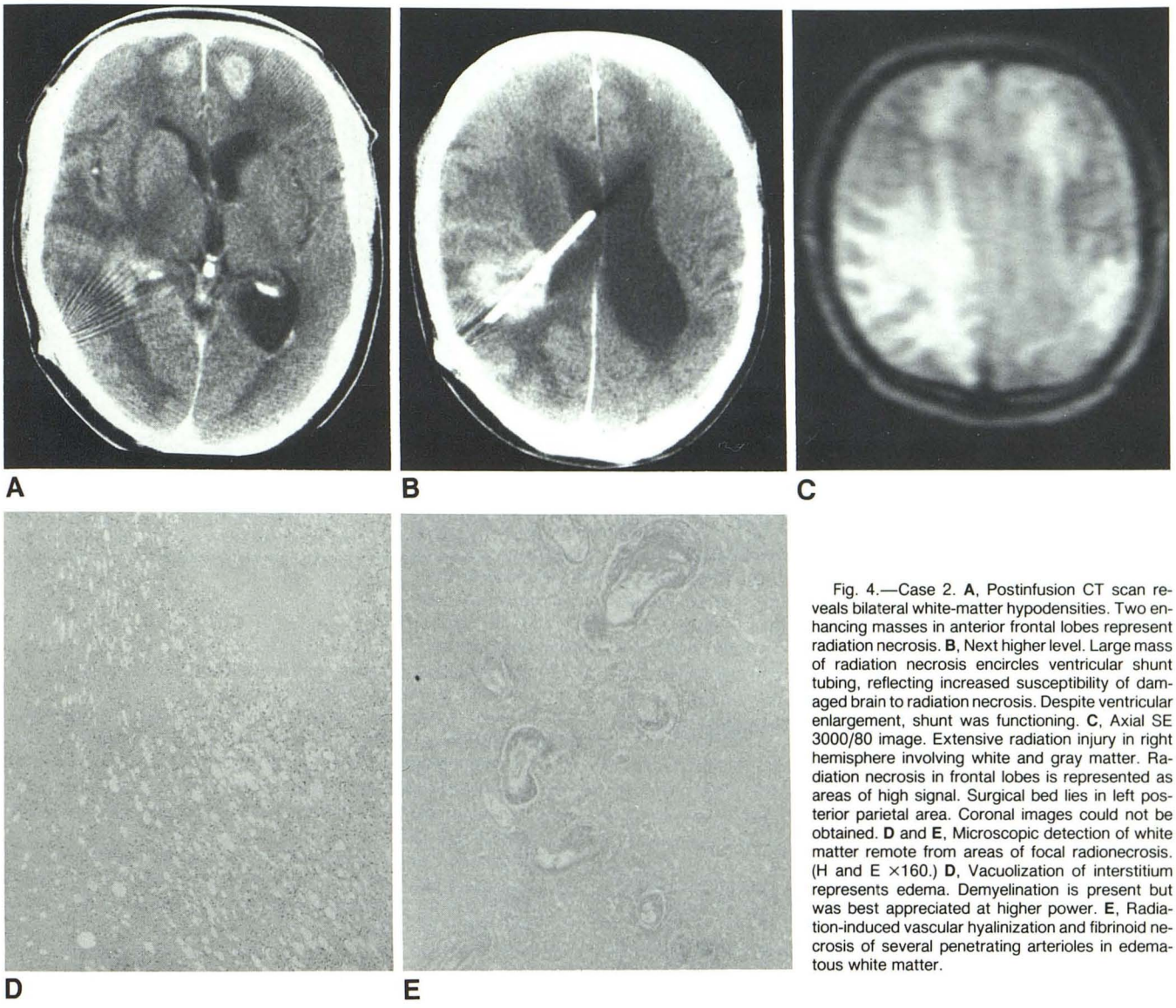

Fig. 4.—Case 2. **A**, Postinfusion CT scan reveals bilateral white-matter hypodensities. Two enhancing masses in anterior frontal lobes represent radiation necrosis. **B**, Next higher level. Large mass of radiation necrosis encircles ventricular shunt tubing, reflecting increased susceptibility of damaged brain to radiation necrosis. Despite ventricular enlargement, shunt was functioning. **C**, Axial SE 3000/80 image. Extensive radiation injury in right hemisphere involving white and gray matter. Radiation necrosis in frontal lobes is represented as areas of high signal. Surgical bed lies in left posterior parietal area. Coronal images could not be obtained. **D** and **E**, Microscopic detection of white matter remote from areas of focal radionecrosis. (H and E ×160.) **D**, Vacuolization of interstitium represents edema. Demyelination is present but was best appreciated at higher power. **E**, Radiation-induced vascular hyalinization and fibrinoid necrosis of several penetrating arterioles in edematous white matter.

bral atrophy may resemble communicating hydrocephalus. The diagnosis of hydrocephalus is excluded when gradual ventricular enlargement is coupled with cortical atrophy (Fig. 2), temporal horn enlargement is absent (Fig. 1), or a functioning ventriculoperitoneal shunt is present (Fig. 4).

The adjunctive effect of intravenous methotrexate with cranial irradiation in the production of disseminated necrotizing leukoencephalopathy has been observed in acute lymphocytic leukemia of childhood [9, 10]. Four of our patients received methotrexate, two received carmustine (BCNU), and one cis-platinum. While white-matter disease was not limited to the chemotherapy group, an adjunctive effect may account for the severity of white-matter changes seen on MRI and CT. No patients in our series received chemotherapy without radiotherapy, but investigation of such a group is planned to determine if chemotherapeutic agents produce an independent adverse effect on the white matter.

In a prospective series of 13 patients with small-cell lung carcinoma treated with multiagent chemotherapy and prophylactic cranial irradiation (3000 rad [30 Gy]), CT showed cortical atrophy in all cases with ventricular dilatation in nine and periventricular lucencies in two [11]. Cases 4 and 9 of our study underwent this same treatment. In both cases, CT showed atrophy and ventricular dilatation but normal attenuation of the white matter. However, MRI demonstrated abnormal white-matter signal in both. A prospective study is planned to evaluate further the efficacy of CT versus MRI in this group of patients.

In summary, MRI is superior to CT in the detection of radiation injury, showing abnormal white-matter signal where CT is normal. The coronal SE 1000/80 pulse sequence optimally demonstrates injured, edematous fiber tracts profiled between CSF and gray matter. A scalloped, irregular contour involving the more posterior fiber tracts distinguishes this

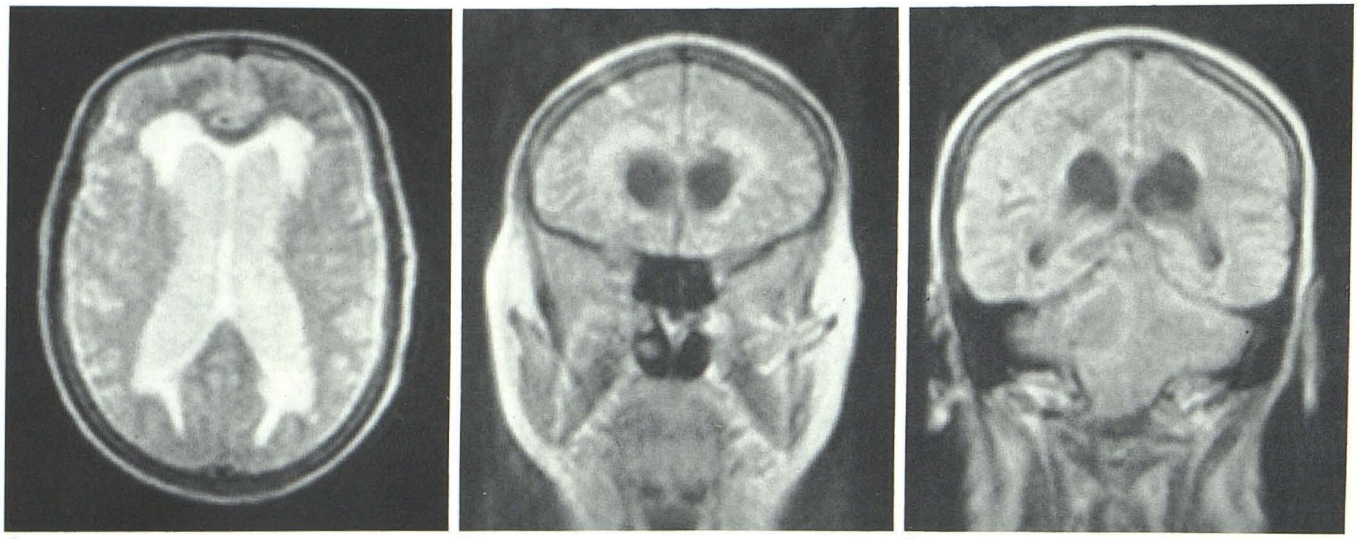

Fig. 5.—Obstructive hydrocephalus secondary to cerebellar hemangioblastoma. **A**, Axial SE 3000/80 image clearly demonstrates bright, rounded periventricular signal representing transependymal absorption. Edema does not extend to gray-white matter junction. **B** and **C**, Coronal SE 1000/80 images poorly demonstrate symmetric, rounded pattern seen in transependymal absorption. Ventricles and temporal horns are enlarged. Posterior white-matter tracts and centrum semiovale appear spared (**C**). (Bright line over right hemisphere is artifact.)

injury from transependymal absorption of hydrocephalus. The underlying cause for this signal is radiation injury to the tenuous blood supply of the white matter, resulting in edema, demyelination, and tissue necrosis.

REFERENCES

1. Mikhael MA. Radiation necrosis of the brain: correlation between patterns on computed tomography and dose of radiation. *J Comput Assist Tomogr* **1979**;3:241–249
2. Kingsley DPE, Kendall BE. CT of the adverse effects of therapeutic radiation of the central nervous system. *AJNR* **1981**;2:453–460
3. Burger PC, Mahaley MS Jr, Dudka L, Vogel FS. The morphologic effects of radiation administered therapeutically for intracranial gliomas. A postmortem study of 25 cases. *Cancer* **1979**;44:1256–1272
4. Jackson JA, Leake DR. Schneiders NJ, et al. Magnetic resonance imaging in multiple sclerosis: results in 32 cases. *AJNR* **1985**;6:171–176
5. Courville CB, Myers RO. The process of demyelination in the central nervous system. II. Mechanism of demyelination and necrosis of the cerebral centrum incident to x-radiation. *J Neuropathol Exp Neurol* **1958**;17:158–181
6. Di Chiro G, Arimitsu T, Brooks RA, et al. Computed tomography profiles of periventricular hypodensity in hydrocephalus and leukoencephalopathy. *Radiology* **1979**;130:661–666
7. Cowley RA. Influence of fiber tracts on the CT appearance of cerebral edema: anatomic-pathologic correlation. *AJNR* **1983**;4:915–925
8. Dooms G, Brant-Zawadzki M, Hecht S, et al. The MRI appearance of radiation effects in the brain. Presented at the annual meeting of the American Society of Neuroradiology, New Orleans, February **1985**
9. Lee Y-Y, Glass JP, van Eys J, Wallace S. Medulloblastoma in infants and children: computed tomographic follow-up after treatment. *Radiology* **1985**;154:677–682
10. Peylan-Ramu N, Poplack DG, Pizzo PA, Adornato BT, Di Chiro G. Abnormal CT scans of the brain in asymptomatic children with acute lymphocytic leukemia after prophylactic treatment of the central nervous system with radiation and intrathecal chemotherapy. *N Engl J Med* **1978**;298:815–818
11. Craig JB, Jackson DV, Moody D, et al. Prospective evaluation of changes in computed cranial tomography in patients with small cell lung carcinoma treated with chemotherapy and prophylactic cranial irradiation. *J Clin Oncol* **1984**;2:1151–1156